RPN55

INTENSE RELATIVISTIC ELECTRON BEAM-PLASMA INTERACTIONS IN FINITE CAVITIES

PIIR-29-71

June 1971

by

Sidney Putnam

Presented at the Eleventh Symposium on
Electron, Ion, and Laser Beam Technology
Boulder, Colorado, May 1971

Physics International Company
2700 Merced Street
San Leandro, California 94577

CONTENTS

ILLUSTRATIONS

SECTION 1
INTRODUCTION

The propagation of intense relativistic electron beams in neutral gas-filled drift chambers has been studied experimentally during the past several years. Depending on gas pressure and beam parameters, one observes, for example, regions of ion acceleration, relatively efficient beam transport, or highly unstable behavior (Reference 1). In order to understand these different regimes, it is necessary to consider, in addition to the beam dynamics, the time-varying electromagnetic (EM) beam cavity interactions with boundary conditions appropriate to experimental geometries. The full self-consistent problem is extremely complex, involving charge production processes and coupled EM-orbit equations, and is probably ultimately amenable only to numerical solution. Nevertheless, most of the gross beam behavior can be understood with simple models.

In this paper we discuss EM fields generated by beams in finite cavities and outline a procedure to calculate charge production in neutral gases that gives gas breakdown times in agreement with the data of Yonas and Spence (Reference 2). The electrostatic field effects on low-pressure beam propagation are considered in some detail and a model for predicting transverse instability wavelengths is also given. Throughout the discussion the emphasis is upon simple formulations of the important beam physics, which will hopefully be of use for practical application.

SECTION 2
ELECTROMAGNETIC FIELDS IN FINITE CAVITIES

2.1 QUASI-STATIC MODEL FIELDS BEFORE GAS BREAKDOWN

We first develop expressions for the EM fields in closed conducting cavities which include the effects of cavity end plates, variations in beam radius, charge/length, and density of background charge. Plasma effects are included only in terms of electrical (space charge) neutralization. The geometry is shown in Figure 2.1. Azimuthal symmetry is assumed as it is that the theta component of the beam current is zero. Direct integration of the Maxwell equation:

$$\nabla \times \vec{E} = -\frac{1}{c}\frac{\partial \vec{B}}{\partial t}$$

gives

$$E_z = -\int_r^R \frac{\partial E_r}{\partial z}\,dr' - \frac{1}{c}\int_r^R \frac{\partial B_\theta}{\partial t}\,dr' \qquad (1)$$

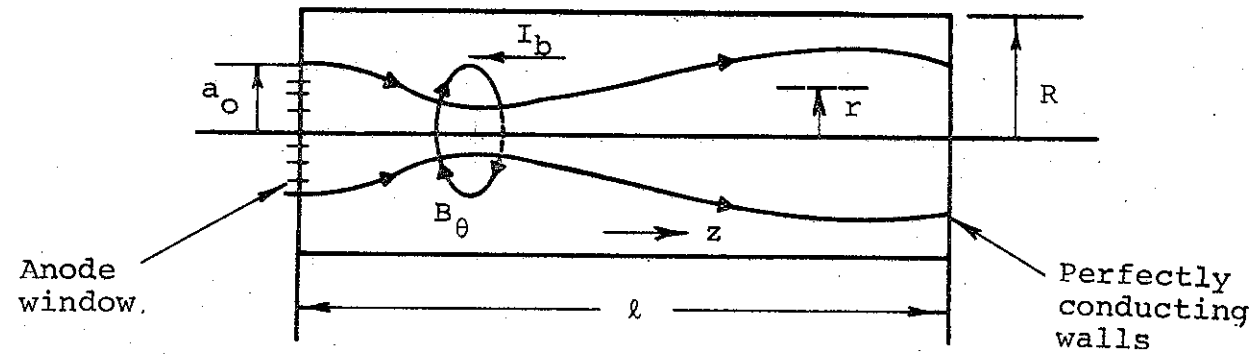

Figure 2.1 Beam chamber geometry.

where the boundary condition $E_z = 0$, $r = R$ has been imposed. In the quasistatic limit, the displacement current in the calculation of B_θ has been neglected and the radial electric field is assumed to be obtainable from the electrostatic (ES) potential. It is thus required that the time for light to travel twice the longest chamber dimension be small compared to times of interest. The ES potential can be determined exactly:

$$\Phi = \int_0^R r'\,dr' \int_0^\ell dz'\, G(r,r',z,z')\rho(r',z') \qquad (2)$$

with

$$G(r,r',z,z') = \frac{8\pi}{R} \sum_{n=1}^{\infty} \frac{J_o\left(\frac{\lambda_n r}{R}\right) J_o\left(\frac{\lambda_n r'}{R}\right)}{\lambda_n \left[J_1(\lambda_n)\right]^2 \sinh\left(\frac{\lambda_n \ell}{R}\right)}$$

$$\begin{cases} \sinh\left(\frac{\lambda_n}{R}\right) z \sinh\frac{\lambda_n}{R}(\ell - z'), & z \leqslant z' \\ \sinh\left(\frac{\lambda_n}{R}\right)(\ell - z) \sinh\frac{\lambda_n}{R} z', & z \geqslant z' \end{cases} \qquad (3)$$

The charge density is $\rho(\text{esu/cm}^3)$ and λ_n are the roots of $J_o(x)$. An ad hoc approximation for E_r is now made to avoid the complications of Equation 2. The spirit of the approximation is to note from the exact expression the term dropping off most slowly in z, and then to find an approximate normalization factor. The chamber radius r is to be restricted to a range such that the z dependence is reasonably accurate for small z. This implies that $1 \leqslant R \leqslant 10$ length units, which is henceforth considered the range for R. Assuming a uniform beam current density,

$$E_r = f(z)\,\frac{2\lambda}{a^2}\,r,\quad r \leqslant a$$

$$= f(z)\,\frac{2\lambda}{r},\quad r \geqslant a \qquad (4)$$

with $f(z) = 0,\ 0,\ \ell$. The beam charge/length (which may also have a z dependence) is denoted by λ. Equation 4 is exact at $z = \ell/2$ for λ constant. Two cases of interest are

$$(1)\quad \ell \lesssim R \longrightarrow f(z) \approx \frac{4z(\ell-z)}{\ell^2}$$

$$(2)\quad \ell > R \qquad (5)$$

$$f(z) \approx \frac{1-e^{-2.4\ z/R}}{(1-e^{-2})},\quad z \lesssim 2(R/2.4)$$

$$= 1,\quad 2(R/2.4) \leqslant z \leqslant \ell - 2R/2.4$$

$$= \frac{1-e^{-2.4\ (\ell-z)/R}}{1-e^{-2}},\quad \ell - 2R/2.4 \leqslant z \leqslant \ell$$

The E_r profile for these two cases are sketched in Figure 2.2.

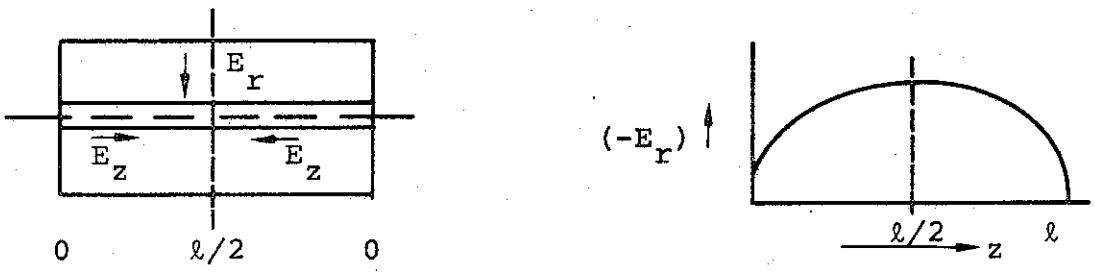

Electrostatic field when $\ell \leqslant R$ Radial field when $\ell \geqslant R$

Figure 2.2 Fields for a uniform electron beam in a closed cavity.

Returning to Equation 1, and using

$$B_\theta = \frac{2I}{ca^2}\, r, \quad r \leqslant a$$

$$= \frac{2I}{cr}, \quad r \geqslant a$$

an expression for $E_z(0,z,t)$ is obtained when $\ell < R$:

$$E_z(0,z,t) = \overbrace{-\,2\,\frac{\partial\lambda}{\partial z}\left(\frac{1}{2} + \mathcal{L}n\left(\frac{R}{a}\right)\right)\frac{4z(\ell-z)}{\ell^2}}^{(1)} + \overbrace{\frac{2\lambda}{a}\,\frac{\partial a}{\partial z}\left(\frac{4z(\ell-z)}{\ell^2}\right)}^{(2)}$$

$$\overbrace{-\,2\lambda\left(\frac{1}{2} + \mathcal{L}n\left(\frac{R}{a}\right)\right)\frac{4}{\ell^2}\,(\ell-2z)}^{(3)} - \overbrace{\frac{2}{c^2}\,\frac{\partial I}{\partial t}\left(\frac{1}{2} + \mathcal{L}n\left(\frac{R}{a}\right)\right)}^{(4)}$$

$$\overbrace{+\,\frac{2}{c^2}\,\frac{I}{a}\,\frac{\partial a}{\partial t}}^{(5)} \qquad (6)$$

If $R > \ell$, a similar evaluation for E_z can be made using Equation 5.

The terms of Equation 6 can be identified as follows:

(1) Electrostatic due to a variation in beam charge density/length modulated by end plate surface charges

(2) Electrostatic due to a variation of beam radius with z modulated by end plate surface charges

(3) Electrostatic due to induced (positive) surface charges at the end plates which terminate the field lines of adjacent beam (negative) charges

(4) Changing magnetic flux due to current variation (L dI/dt)

(5) Changing magnetic flux due to containment of current within a time varying radius (I dL/dt)

It is interesting to note that, without end plates (set $z = \ell/2$), Equation 6 reduces to

$$E_z(0,z,t) = \frac{2}{\gamma_L^2} \frac{\partial \lambda}{\partial u} \left(\frac{1}{2} + \ell n \left(\frac{R}{a} \right) \right), \qquad (7)$$

(no end plates)

$$u = \beta_L ct - z$$

$$\gamma_L = 1/\sqrt{1-\beta_L^2}$$

$\beta_L c$ = forward streaming velocity of beam electrons

if not referring to the beam head or tail and if a constant beam radius with varying charge/length is assumed. If we are within the current rise portion of a beam of electrons ($\partial\lambda/\partial u < 0$) streaming in the positive z direction, E_z is in the negative z direction (i.e., in a direction to accelerate the front electrons) and is opposite in sign to the E_z field behind the head when the beam emerges from a conducting end plate. Equation 7 can be rewritten

$$E_z\Big|_{r=0} \text{ (V/cm)} = \frac{(-)4}{\gamma^2 \beta_L^2} \frac{I^P(\text{amps})}{t_r(\text{nsec})} \left(\frac{1}{2} + \ell n\ R/a\right) e^{-\alpha u} \quad (8)$$

where $I_b = I^P(1-e^{-\alpha u})$ and (α^{-1}) is defined as a two e-folding length:

$$\alpha \beta_L c t_r = 2$$

For $I^P = 5\text{x}10^4$ amps, $t_r = 20$ nsec, $\gamma = 3$, $R = 6$, $a = 1$ and $\beta_L \simeq 0.8$, $E_z \simeq 4\text{x}10^3\ e^{-\alpha u}$ V/cm.

The effects of ions at rest can easily be included in the above equations by replacing λ by $\lambda(1-f_e)$; $f_e \equiv \rho_{ion}/\rho_{electron}$ is the fractional electrical neutralization.

If we take $f_e = f_e(u)$, then Equation 6 gives for constant beam radius:

$$E_z(0,u) = +2\left(\frac{1}{2} + \ell n\ R/a\right) \left[\frac{\partial \lambda}{\partial u}\left(\frac{1}{\gamma_L^2} - f_e\right) - \lambda \frac{\partial f_e}{\partial u}\right] \quad (9)$$

and E_z reverses sign when

$$\lambda \frac{\partial f_e}{\partial u} = \left(\frac{1}{\gamma_L^2} - f_e\right) \frac{\partial \lambda}{\partial u} \quad (10)$$

If both λ and f_e increase linearly behind the beam front, Equation 10 is satisfied when $f_e = 1/2\gamma_L^2$. Figure 2.3 shows qualitatively the effects of ions upon E_z.

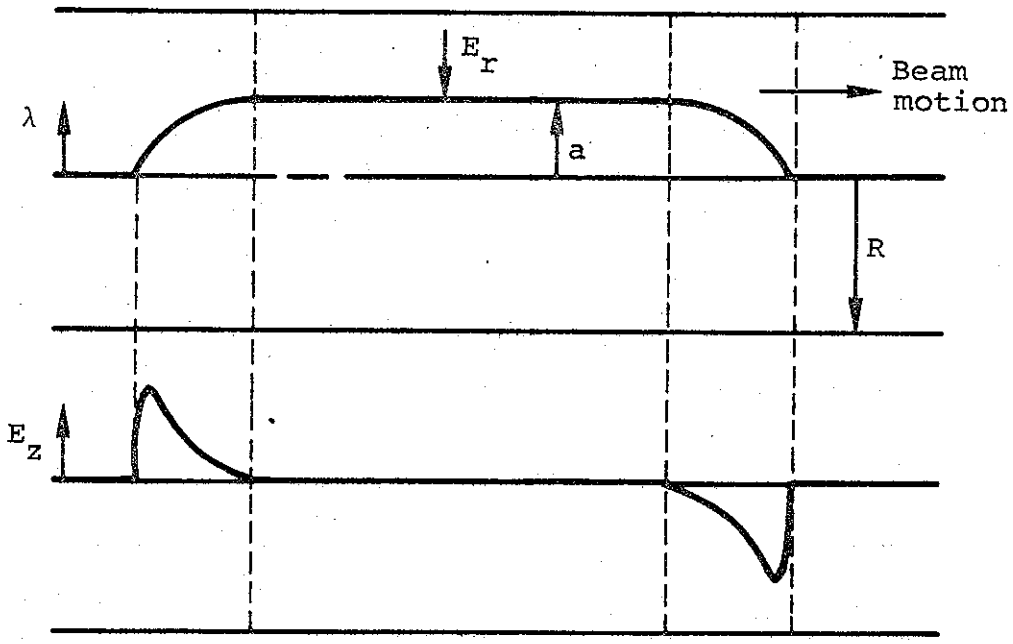

Long conducting pipe, no ions, $f_e = 0$

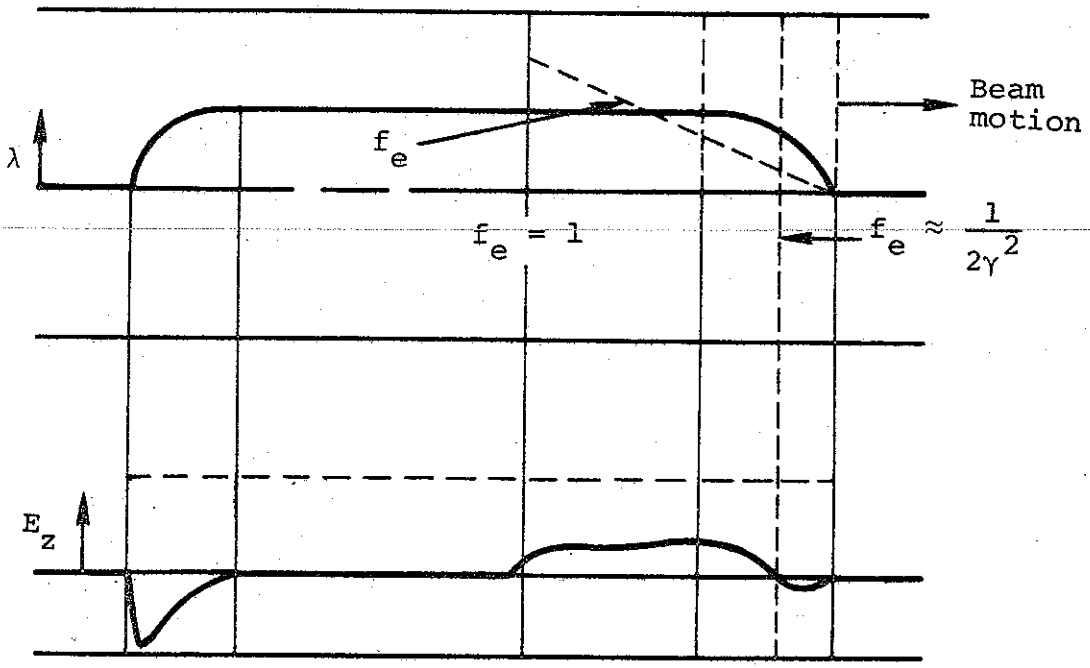

Long conducting pipe, f_e increases linearly behind beam front.

Figure 2.3 Sketches of E_z fields with and without ions.

After $f_e = 1$, only the inductive components of E_z remain and the end plates can be ignored. Thus, for $\tau_N \lesssim t < t_B$; i.e., the time between electrical neutrality, τ_N, and gas breakdown, t_B,

$$E_r \approx 0$$

$$E_z(0,z,t) \approx \frac{2}{c^2}\frac{dI}{dt}\left[\frac{1}{2} + \ell n(R/a)\right] + \frac{2}{c^2}\frac{I}{a}\frac{da}{dt} \qquad (11)$$

If the beam radius is approximately constant, Equation 11 reduces to

$$E_z(V/cm) \quad \frac{2I^P(amps)}{t_r\ (nsec)}\left(\frac{1}{2} + \ell n\ R/a\right) \qquad (12)$$

for $I = I^P \frac{t}{t_r}$, $t \leq t_r$.

2.2 FIELDS AFTER GAS BREAKDOWN

The time scale for changes in the magnetic field or the net current after gas breakdown is the magnetic diffusion time, t_d, which is defined as the time for the field to diffuse a distance of the order of the beam radius:

$$t_d \approx \frac{4\pi\sigma a^2}{c^2} \qquad (13)$$

with the conductivity (sec^{-1}) after breakdown. When t_d is much longer than the remaining beam pulse width, the net current is approximately constant and an estimate of E_z can be obtained by assuming that $I_{net}\ (t > t_B) \approx I_{beam}\ (t=t_B)$, giving

$$E_z \simeq \frac{I_b(t) - I_b(t=t_B)}{\pi a^2 \sigma} \qquad (14)$$

This field places a limit on beam transport efficiency for times after breakdown or for beams injected into preionized plasmas. For example, in an external B_z plasma system with a conductivity of 100 mho/cm, corresponding to a fully ionized hydrogen plasma of a few volts temperature, a beam with current density of 10^5 amp/cm^2 would lose 100 keV/meter of transport.

We have now outlined procedures to estimate EM fields at all times of interest for intense beams injected into neutral gases. We have assumed that the beam current profiles were specified and have not considered orbit or beam envelope dynamics. The utility of the equations for beam transport problems is, of course, that one can set up EM limits on beam transport efficiency for desired beam and chamber parameters. Moreover, if E_z is small enough that the beam streaming velocity does not change appreciably over distances of interest, beam envelope equations such as the Kapchinskij-Vladimirskij equation (Reference 3), which do not consider E_z field effects, can be applied with confidence.

2.3 EXACT EM SOLUTIONS FOR BEAM PENETRATING AN END PLATE IN A FINITE RADIUS CHAMBER

The discussion above assumes that the beam has already traversed the drift chamber. Now to be considered are exact solutions to Maxwell's equation for a beam penetrating a chamber end plate; sufficient conditions will be presented to justify neglect of end plate effects. The material discussed is of interest for low-pressure beam transport in ion acceleration modes when electrostatic fields dominate, and it shows the importance of finite chamber boundaries. The details of the calculations are given in Reference 4.

An end plate has two effects on the EM fields. One, primarily electrostatic, is to reverse the direction of E_z near the end plate and short out the radial electric field. The other is to generate a radiated field component as surface charges are accelerated by the beam. This field gives rise to precursor fields traveling at the velocity of light and, under certain conditions, to oscillatory fields near the beam front. The geometry for the calculations is shown in Figure 2.4.

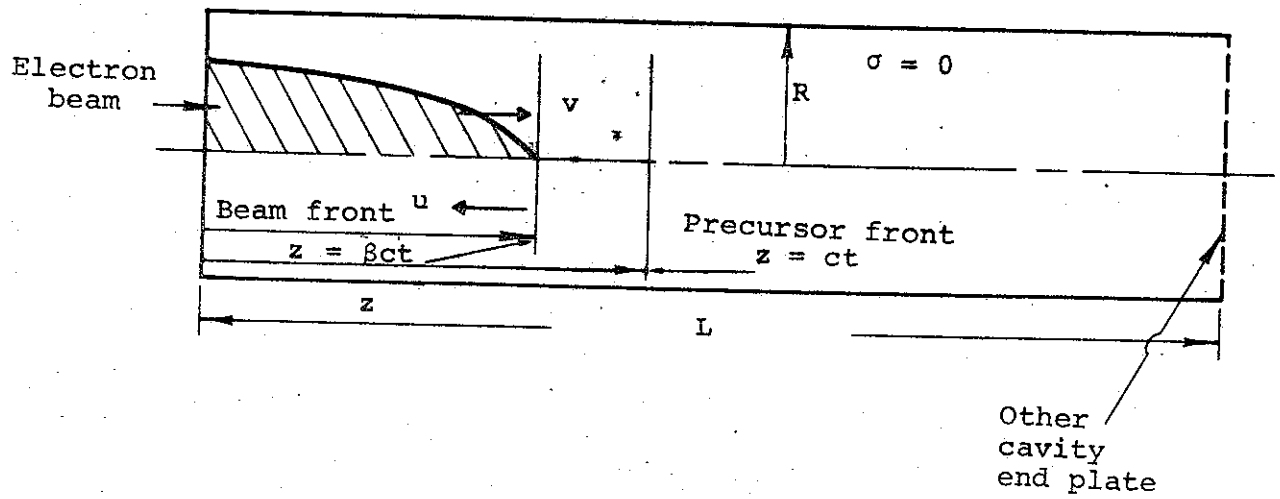

Figure 2.4 Open ended pipe geometry.

A sufficient criterion for neglect of field oscillation is that

$$\sqrt{(ct)^2 - z_f^2} >> R/2.4, \quad 1 \lesssim R \lesssim 10 \text{ length units} \qquad (15)$$

where z_f is the beam front position. Another way of stating Equation 15 is that the light signal must have traveled "far beyond" the beam front. One would therefore not expect this

effect to be important for low-energy beams. A typical oscillation amplitude, for example, would be $\sim 10^3$ V/cm with 5×10^4 A 1-MeV beam, 20-nsec risetime, and 1-cm radius in a 6-cm-radius pipe.

The reversal of the sign of E_z, as compared to the case without end plates, is perhaps the most important influence of the end plate, since this effect can seriously degrade the beam energy and reduce the front velocity. The beam "blows up" radially, resulting in large energy losses. Figures 2.5, 2.6 and 2.7 show the E_z field on axis for a beam with current in the positive z direction penetrating an end plate. In order to illustrate the details of the ES field near the end plate, a "slow" beam was chosen. The parameters are

$$\beta_L \simeq 1/30$$

$$t_r \simeq \text{risetime} \simeq 0.1 \text{ nsec}$$

$$R = 6 \text{ cm}$$

$$a \simeq 1 \text{ cm (Gaussian radial current variation)}$$

$$I^P = \text{peak current} \simeq 1.77\times10^3 \text{ amperes}$$

The reversal of the sign of E_z occurs at the crossover distance, z_c, and can be estimated from

$$z_c \approx (R/2.4\ \ell n\ 2\gamma + \gamma z_f)/\gamma + 1, \qquad (16)$$

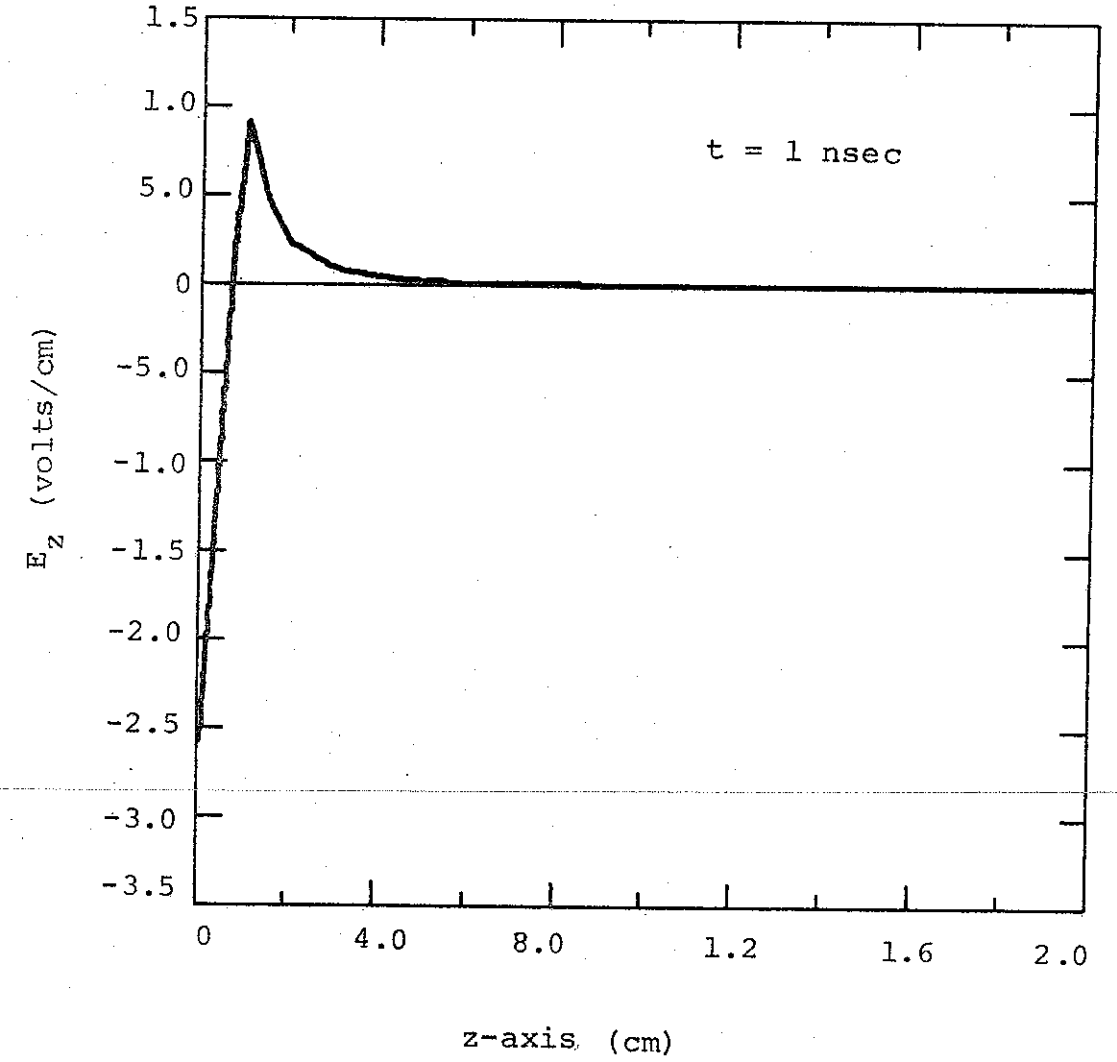

Figure 2.5 The longitudinal electric field (E_z) on axis for a beam penetrating an end plate in a finite radius cavity (t = 1 nsec).

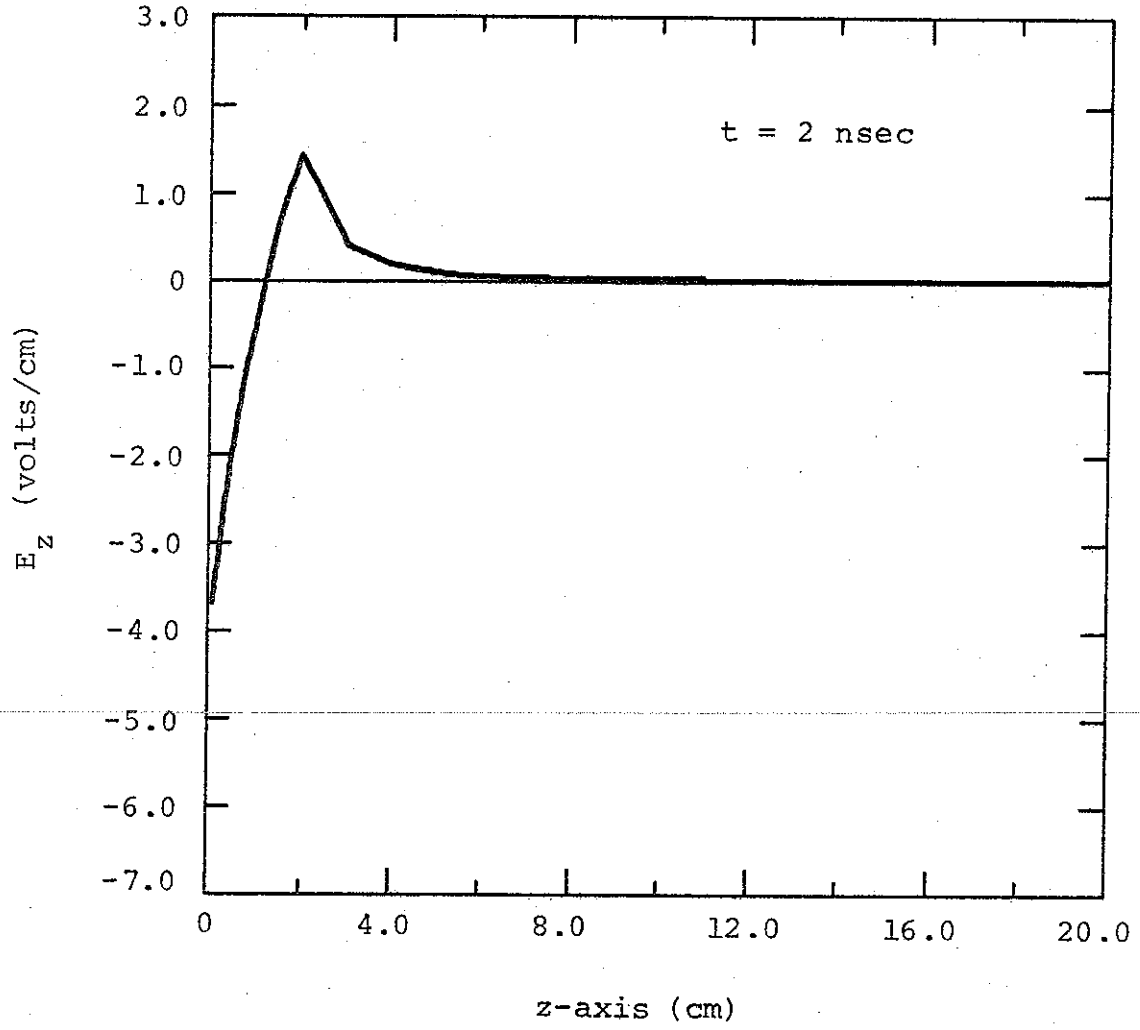

Figure 2.6 The longitudinal electric field (E_z) on axis for a beam penetrating an end plate in a finite radius cavity (t = 2 nsec).

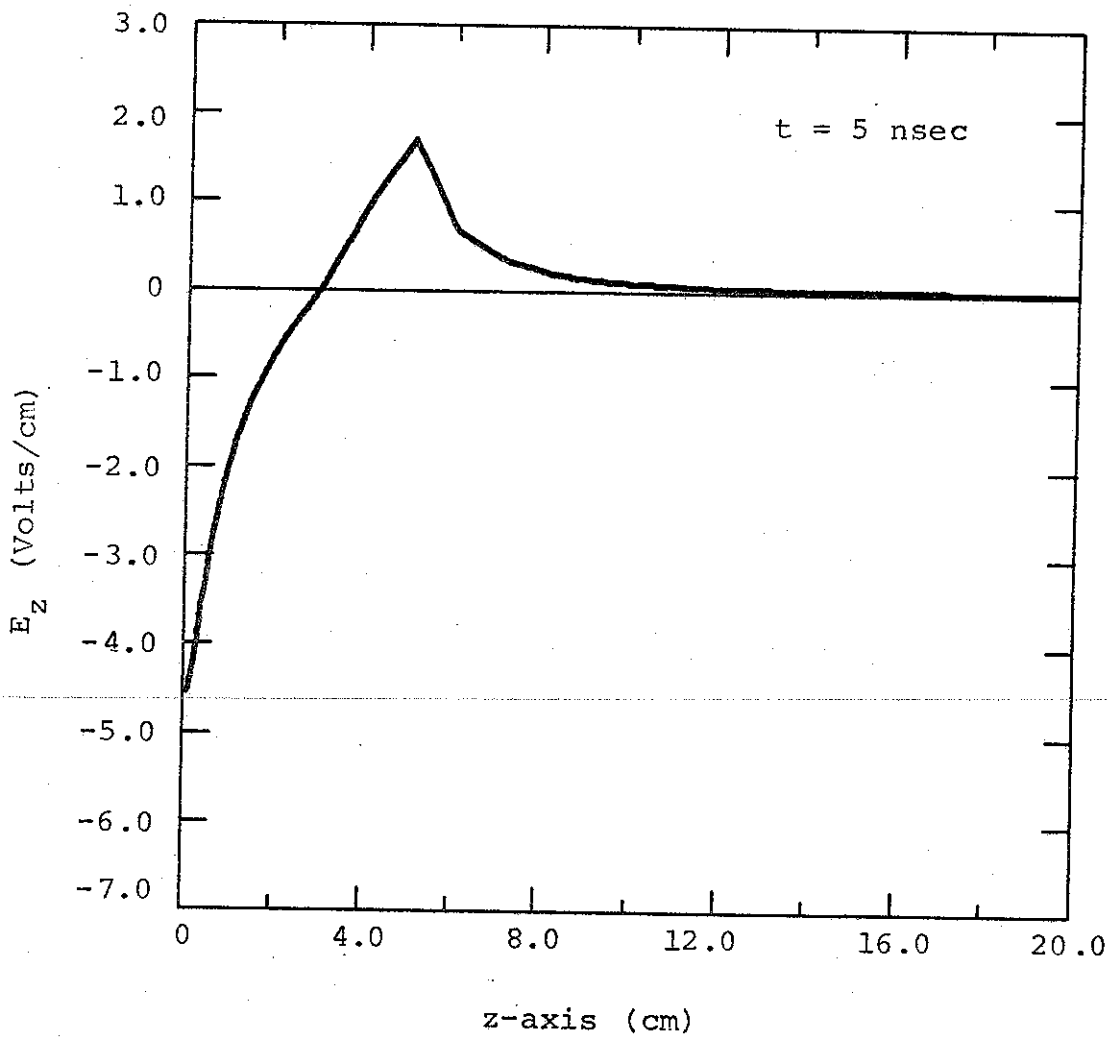

Figure 2.7 The longitudinal electric field E_z on axis for a beam penetrating an end plate in a finite radius cavity (t = 5 nsec).

where z_f is the beam front position ($\approx$ time in nanoseconds in the above example). Equation 16 is valid for a "blunt" beam when $z_c \lesssim 2R/2.4$. In order to neglect the electrostatic end plate effect on the beam fields, it is required that

$$z_f,\ z >> R/2.4\ \ell n\ 2\gamma \tag{17}$$

When $R \longrightarrow \infty$, one can also derive a manageable expression for the E_z field:

$$E_z(0,z,z_f) = -\frac{2\lambda}{a^2}\left\{2(z_f-z) + 2\sqrt{a^2+z^2} - \sqrt{a^2+(z_f-z)^2} - \sqrt{a^2+(z_f+z)^2}\right. \tag{18}$$

and a transcendental equation for z_c is obtained by setting E_z in Equation 14 equal to zero.

SECTION 3
LOW PRESSURE BEAM PROPAGATION

When the electrical neutralization time, τ_N, is $\lesssim t_p$, the beam pulse width, electrostatic effects dominate beam propagation. We can estimate the electrostatic potential well depth, ϕ, for a beam penetrating a cavity as being approximately

$$\phi \text{ (volts)} \approx \frac{60\ I_{(amps)}}{\beta_L} (1/2 + \ell n\ R/a)(1-e^{2.4\ z_c/R})$$

$$z_c \lesssim 2(R/2.4)$$

$$1 \lesssim R \lesssim 10 \text{ length units} \qquad (19)$$

If $\phi\ (z_c) << $ beam kinetic energy, the beam propagation will not be limited by the longitudinal electrical field, although space charge effects on radial motion must still be considered. If, however, $\phi\ (z_c) \geqslant$ beam kinetic energy, a length, $\bar{z}_c$, is defined by $\phi\ (\bar{z}_c)$ = kinetic energy and if the exponential factor in Equation 19 is approximated by a straight line,

$$\bar{z}_c \text{ (cm)} \approx \frac{3.4\text{x}10^4}{I^P \text{ (amps)}} \left(\frac{t_r}{t_v}\right) \frac{\sqrt{1 + V^P}\ \sqrt{V^P}}{(1 + 2V^P)}$$

$$R/2.4 \left(\frac{1}{1/2 + \ell n\ R/a)}\right),\ \bar{z}_c \lesssim 2\ (R/2.4) \qquad (20)$$

where V^P = peak electron kinetic energy in MeV, t_r is the current risetime, t_v is the electron kinetic energy risetime, and I^P is the peak beam current. The voltage and current rise have been taken as linear, and $\beta_L \simeq \beta$. If $I^P \simeq 30$ kA, $t_r/t_v \simeq 2$, $V^P \approx 1$ MeV, $R \simeq 6$ cm, and $a = 1$, then $z_c \approx 1.2$ cm. One can estimate a front velocity $(\beta_f c)^{ES}$ by assuming that the front travels a distance, $\bar{z}_c$, over a time scale of τ_N:

$$\beta_f^{ES} \simeq \frac{\bar{z}_c}{c\tau_N} \tag{21}$$

This velocity is very slow for high ν/γ beams and places a severe constraint on high ν/γ beam propagation efficiency at low pressures. Ion acceleration, as proposed by Rostoker (Reference 5), is due to the ES field near the beam front. The front velocity accelerates, as τ_N in Equation 21 is effectively decreased by preionization ahead of the beam front.

The discussion of the longitudinal ES field suggests a qualitative picture of the beam-front velocity behavior at low pressures above the ion acceleration cutoff. According to Equation 21, the beam front moves slowly until the charge neutralization front has passed $z \approx 2(R/2.4)$. Then the end plate effect disappears and the front velocity should increase. The front velocity, however, will still be less than βc and will now depend on the "sharpness" of both the beam front and the space-charge neutralization front. As the beam approaches the downstream end plate, an increase in front velocity is again to be expected since the field will reverse direction as ES force lines start to terminate on the surface charges of the end plate.

SECTION 4
CHARGE PRODUCTION

In order to achieve reasonable beam transport efficiency, background gas pressure must be such that breakdown occurs over times < t_r. A model of charge production is now argued to estimate breakdown times and current neutralization. Secondary electron orbit sketches and typical field magnitudes are shown in Figure 4.1 for a beam in a drift chamber. We assume that the beam front is far away from the chamber end plates ($z_f >> 2R/2.4$). Two processes contribute to background gas ionization: direct collisional ionization by the beam electrons and avalanching of secondary electrons by the electric field in appropriate E/P ranges, P being the gas pressure. From Figure 4.1, it can be noted that beam-driven electric fields vary several orders of magnitude from the time of front arrival to gas breakdown time, t_B, and that the highest fields exist for $t \leq \tau_N$. In fact, these fields are usually sufficiently high at pressures of interest (0.1 to 1 torr) that the secondary electrons become relativistic over distances of the order of the beam radius and the ionization cross section drops to values around $\sim 10^{-18}$ cm^2. This can be compared to typical Townsend discharge theory where cross sections are used for electrons with energies up to the kilovolt range ($\sim 10^{-16}$ cm^2 cross section). Moreover, until $f_e \simeq 1$ is achieved, the secondary electron motion is primarily radial and the flow is out of the beam channel. Thus, it seems reasonable to neglect avalanching in the beam channel until $f_e \simeq 1$. When $t > \tau_N$, $|E| \simeq E_z \simeq 10^3$ V/cm, (typically), we consider avalanche

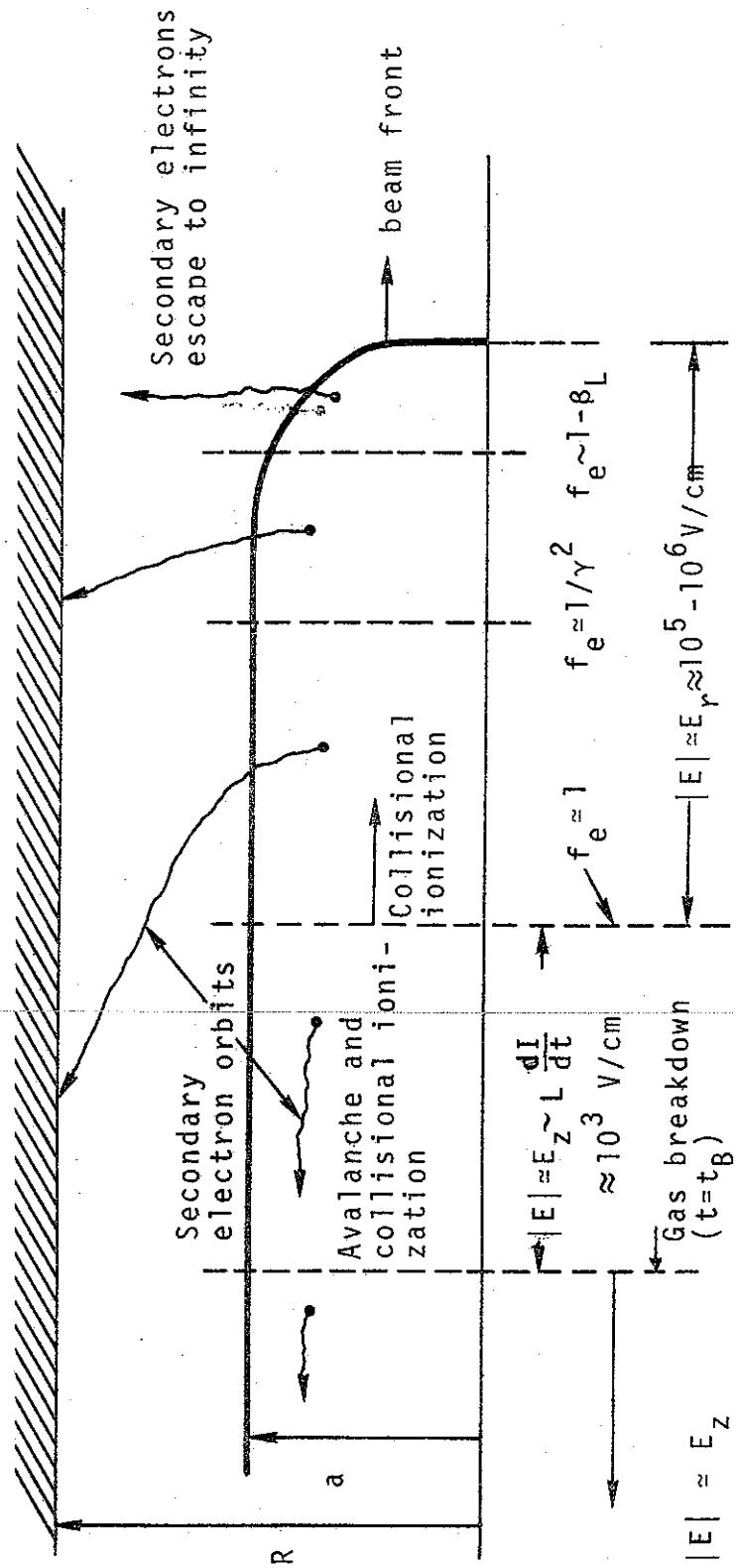

Figure 4.1 Phenomenology of charge production in neutral gas.

effects to be important and, as shown in the previous discussion, the electric field is inductive. With these arguments in mind, an ad hoc charge production calculation procedure for high current electron beams is outlined:

a. τ_N, the time for $f_e \approx 1$, is calculated from collisional ionization (τ_N (nsec) $\cong 0.7/\beta_L P$ (torr) for air).

b. From the time the beam front arrives at the point of interest up to $t = \tau_N$, secondary electrons escape instantaneously out of the beam channel; no significant electron avalanching occurs within the beam channel.

c. From $t = \tau_N$ to $t = t_B$, the breakdown time,

$$E_z \text{ (V/cm)} \approx \frac{2I^P \text{ (amps)}}{t_r \text{ (nsec)}} \quad (1/2 + \ell n\ R/a),$$

assuming a linear current rise,

R = chamber radius
a = beam radius
t_r = beam risetime

Using E_z above and the pressure of interest, t_i, the mean ionization time (Townsend discharge theory), can be determined.

d. Equation of charge production:

$$\frac{dn_e^s}{dt} = \underbrace{\frac{\alpha I(t)}{\pi a^2}}_{\text{collisional ionization}} + \underbrace{\frac{n_e^s}{t_i}}_{\text{avalanche}} - \underbrace{\nabla \cdot \vec{\Gamma}}_{\text{transport}}$$

$\alpha = 5.8 \times 10^{17} P \text{ (torr)}$ for air,
n_e^s = secondary electron number density

Neglecting the transport term and assuming E_z constant,

$$n_e^s (t - \tau_N) = \frac{I^P}{\pi a^2} \left(\frac{t_i}{t_r}\right) \left[e^{t-\tau_N/t_i} (t_i + \tau_N) - (t + \tau_N) \right]$$

e. Breakdown is defined as $n_e^s (t_B) = \delta n_b (t_B)$
Empirically determined $\delta \approx 226$

f. t_B is obtained from the transcendental equation:

$$\frac{e^{t_B - \tau_N/t_i}}{t_B} \approx \frac{80}{P \text{ (torr)}} \frac{1}{t_i \beta_L} \frac{1}{(t_i + \tau_N)} \quad \text{for air}$$

(All times are in nanoseconds.)

A plot of E/P versus P_{t_i} for air is shown in Figure 4.2.

Breakdown time calculations from the above are compared with the Yonas and Spence data in Table 4.1. The beam parameter range over which the above model is relevant is not

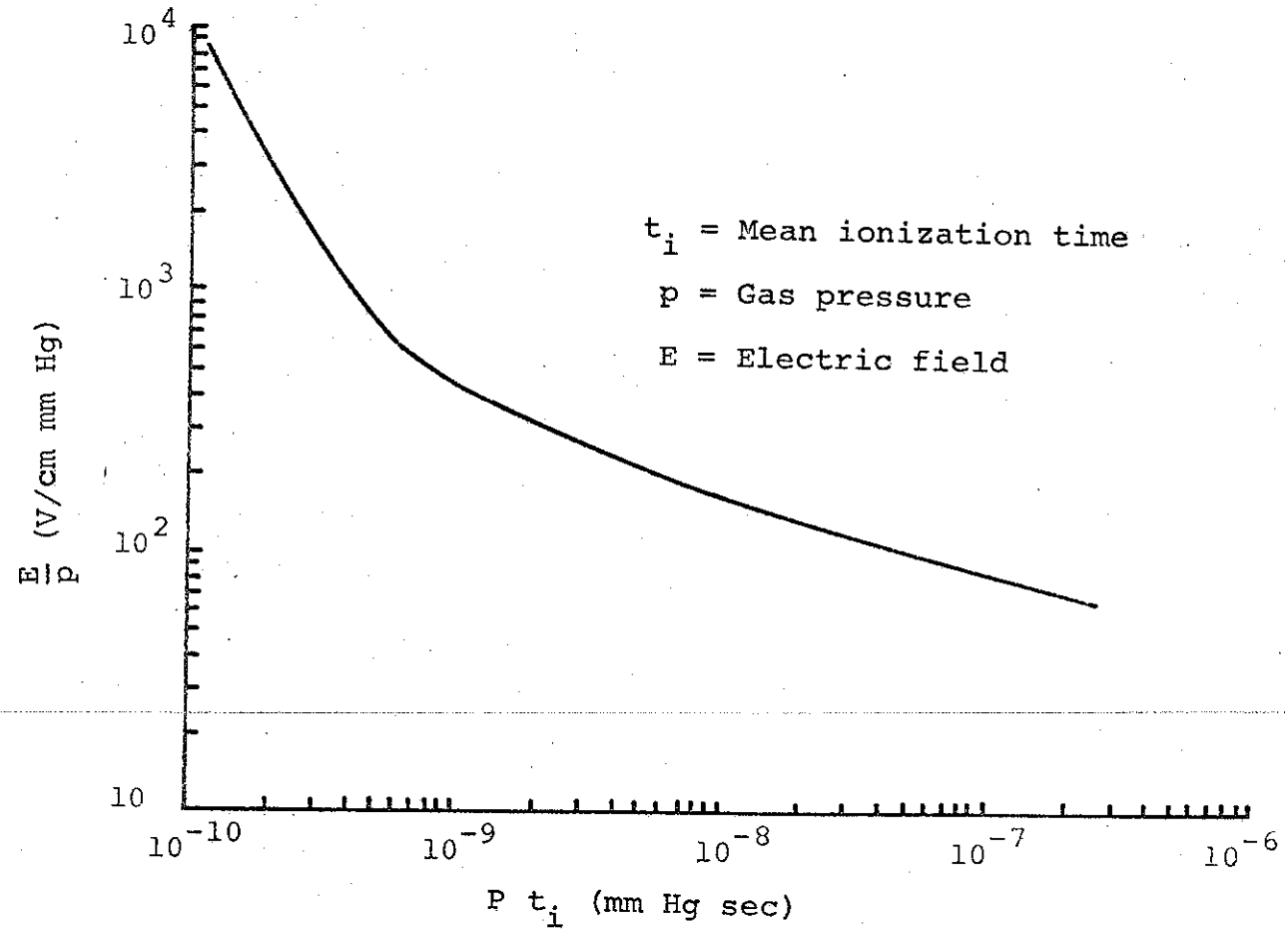

Figure 4.2 Plot of E/p versus p t_i for air.

TABLE 4.1
BREAKDOWN TIME CALCULATIONS

P (torr)	τ_N (nsec)	t_i (nsec)	t_B (nsec) Calculated	t_B (nsec) Measured
0.1	13.0	1.0	20.7	20
0.3	4.3	0.47	7.8	10
0.5	2.6	0.34	5.1	5

Agreement is within experimental error

Parameters

$I^P = 4 \times 10^4$ amperes

$t_r = 20$ nsec

$E_Z = 2 \times 10^3$ volts/cm

$a^2 = 2.5$ cm^2

$\beta_L = 0.54$

$\gamma = 1.5$

$R = a$

clear, inasmuch as detailed breakdown data exists only from the Yonas and Spence work. It is quite likely that widely different beam parameters would require adjustment of the charge multiplication factor, δ.

SECTION 5
TRANSVERSE INSTABILITY

Intense relativistic beams exhibit strong transverse instabilities in appropriate pressure ranges. A typical time-integrated, pinched beam self-photo at 0.1 torr is shown in Figure 5.1; the beam electrons appear to follow a hose-like plasma channel. This behavior is to be contrasted with the transversely unstable, high-pressure ($P > \sim 100$ torr) propagation where the beam is also pinched, but appears to rapidly blow up into a smeared, filamentary structure. Although current neutralization is small for both pinched modes, the plasma conductivity is high at low pressures ($\sigma \overset{>}{\sim} 10^{13} - 10^{14}$/sec) and very low at high pressures because of the high electron plasma collision frequency. The differences in the plasma conductivity suggest markedly different growth-time regimes for transverse instabilities. In the low pressure case, the high plasma conductivity after breakdown gives rise to a velocity dependent drag force on beam "whipping" arising from the resistance of the plasma to motion of the magnetic lines of force as the beam undergoes displacement. When the angular frequency of the perturbation is much less than the plasma conductivity $\sigma(\text{sec}^{-1})$, or when the skin depth of the magnetic field penetration of the plasma is of the order of a few beam radii or less, we adopt the conventional terminology (Reference 6) and refer to the instability as resistive. Thus, before gas breakdown in the low pressure mode, the instability is nonresistive and, after breakdown, resistive. In the high pressure case, a nonresistive mode would apply throughout the beam pulse.

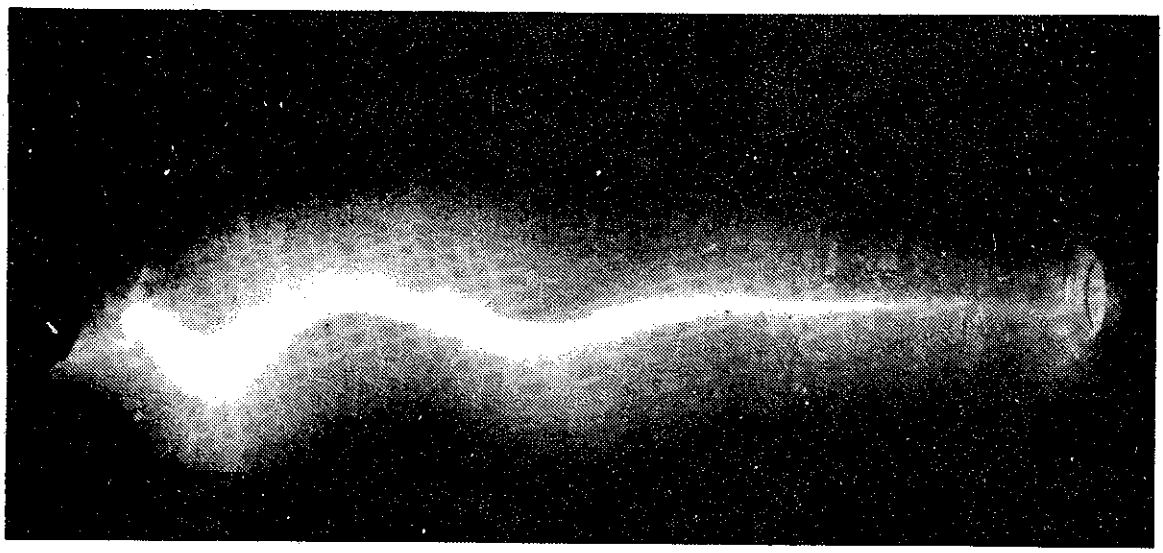

Instability wavelength is approximately 16 cm. Beam parameters: pressure 0.1 torr; beam current approximately 25 kA; average kinetic energy approximately 3 meV; current risetime approximately 10 nsec. The beam is traveling from right to left in the photo.

Figure 5.1 "Frozen hose" instability of a pinched beam.

Rather idealized theoretical models (Reference 7) for non-resistive growth predict the wavelength of the fastest growing transverse oscillation modes; λ_{inst}:

$$\lambda_{inst} = \frac{\pi}{\sqrt{2}} \left(\frac{\nu}{\gamma}\right)^{-1/2} d, \quad d \ll D$$

$$= \frac{\sqrt{\pi}}{2} \left(\frac{\nu}{\gamma}\right)^{-1/2} D, \quad d \sim D \qquad (22)$$

$$\nu = I \text{ (amps)}/17{,}000\ \beta_L$$

where d(D) is the beam (chamber) diameter. Figure 5.2 and 5.3 show experimentally measured wavelengths, showing reasonable agreement with Equation 22. After gas breakdown, resistive mode theory (Reference 8) suggests a growth rate $\cong (t_d)^{-1}$ where t_d is the magnetic diffusion time (Equation 13). For $\sigma \gtrsim 10^{13}$/sec, $t_d \gtrsim 100$ nsec, and the beam path developed in the nonresistive mode thus appears "frozen" over times of the order of the beam pulse.

To summarize, a procedure is outlined to estimate instability wavelengths for the low pressure case:

- From the charge production rules given in Section 2.2, the gas breakdown time at the pressure of interest can be calculated, and the beam current at breakdown time determined.
- The instability wavelength may be estimated by using the above current value to determine ν in Equation 22.

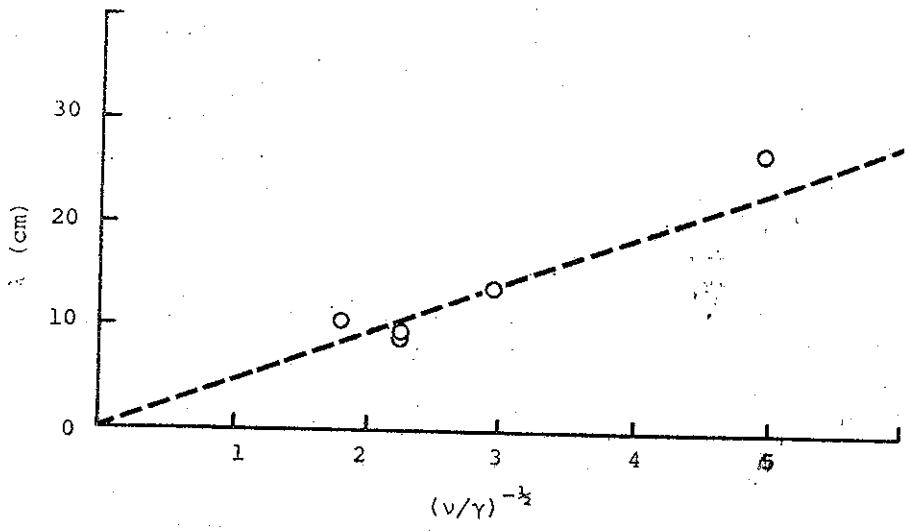

The values of ν/γ are approximate and are obtained from multiple calorimetry. The beam kinetic energy is approximately 3 MeV, the chamber pressure 100 μ, and d = 2 cm.

Figure 5.2 Instability wavelength as a function of $(\nu/\gamma)^{-1/2}$, D << d.

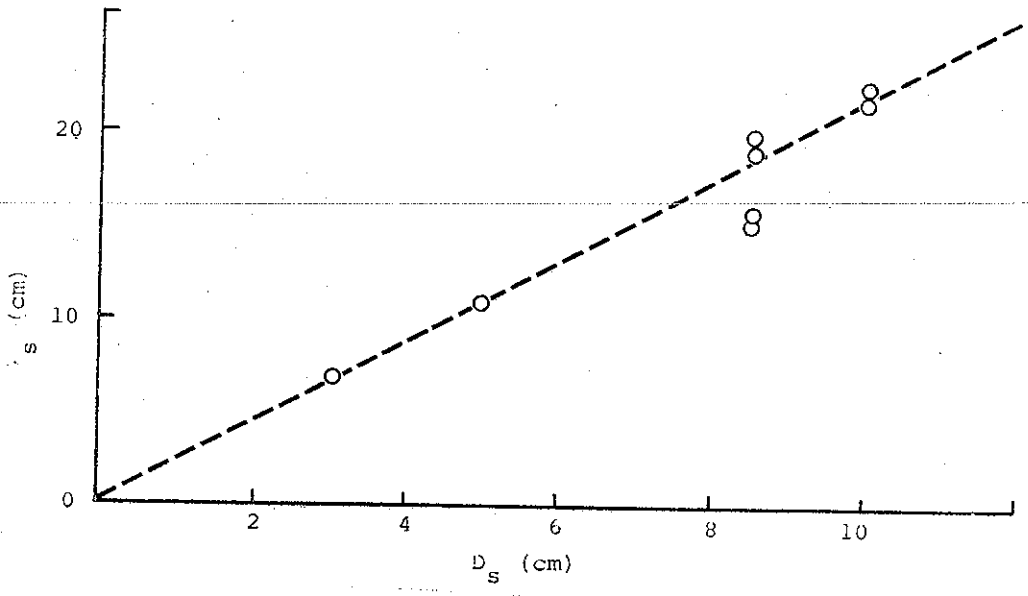

ν/γ is assumed to have the approximately constant value 0.3. The kinetic energy is approximately 3 MeV, the chamber pressure 100 μ.

Figure 5.3 Instability wavelength in guide tube.

REFERENCES

1. S. E. Graybill, "Dynamics of Pulsed High Current Electron Beams," IEEE Transactions on Nuclear Science (June 1971) Proceedings of the March 1971 Chicago National Accelerator Conference.

2. G. Yonas and P. Spence, Record of the 10th Symposium on Electron, Ion and Laser Beam Technology, L. Marton, ed., IEEE Catalog No. 69C22- (1969), p. 443.

3. A. Garren, "Thin Lens Optics with Space Charge," UCRL-19313, Lawrence Radiation Laboratory, Berkeley, California (August 1969(.

4. S. Putnam, "Theoretical Electron Beam Studies," PIFR-105, Physics International Company, San Leandro, California (April 1970).

5. N. Rostoker, "LPS 21," Laboratory of Plasma Studies, Cornell University, Ithaca, New York (July 1969).

6. S. Weinberg, J. Math Physics, 8:614 (1967).

7. D. Finkelstein, P. Sturrock, Plasma Physics, edited by J. Drummond, McGraw-Hill Book Company, New York, N.Y. (1961); B. Chirikov, "Plasma Physics," J. Nuc. Energy, Part C, 8:455 (1966).

8. H. Lewis, "Stability of a Relativistic Beam in a Plasma," IDA Jason Summer Study Group Report (June 1960).